Magnetic Levitation Using Permanent Magnets: System Design, Feedback Stabilization, and Experimental Validation

Dhiraj Basnet and Arash Komaee

Abstract— **This paper presents the design, implementation, feedback stabilization, and experimental validation of a novel permanent magnet levitation system. Conventionally, magnetic levitation systems utilize electromagnets to levitate magnetic objects against gravity by stabilizing them around equilibrium points at which the applied magnetic force balances the gravity. This magnetic force must be dynamically adjusted by means of a stabilizing feedback loop, which is established by easy control of the electromagnet voltage. Despite the key advantage of easier control, electromagnets often produce much weaker magnetic forces compared to permanent magnets of similar size, weight, and cost. Therefore, this paper proposes the use of a permanent magnet to produce the magnetic force necessary for levitation, and the use of a linear servomotor to control the magnitude of this force by adjusting the distance between the magnet and the levitating object. To demonstrate this idea in practice, an experimental setup is designed, prototyped, and successfully stabilized using a computer-based feedback control loop.**

I. Introduction

This paper is a follow-up to our earlier work on the design and development of magnetic levitation systems (MLS) using a combination of permanent magnets and electromechanical actuators [1]–[3]. A conventional MLS usually consists of an electromagnet faced toward the ground to attract a magnetic object against the gravity and levitate it at a point below the face of electromagnet [4] (and references therein). Magnetic levitation is achieved around an equilibrium point at which the attractive magnetic force applied to the magnetic object against gravity balances its weight. This equilibrium point is in essence unstable, and must be stabilized using a feedback control to dynamically adjust the magnetic force applied by the electromagnet via its terminal voltage. The feedback loop is set up by measuring the real-time position of the magnetic object and other relevant variables, which are incorporated then into a stabilizing control applied to the electromagnet.

The basic concept of the MLS developed in this paper was proposed in [1], [2] and is illustrated schematically in Fig. 1. This MLS replaces electromagnets in the existing designs with a magnetomechanical unit consisting of a permanent magnet faced groundward, and a linear servomotor to control its vertical position. This unit is aimed to apply an attractive magnetic force against the gravity, necessary for levitating a magnetic object, and to control the magnitude of this force using the servomotor by adjusting the distance between the permanent magnet and the levitating object. To stabilize the proposed MLS, the reference signal to the servomotor is generated by a feedback controller.

The fusion of permanent magnets and electromechanical actuators is the keystone of our broader work on *noncontact magnetic manipulators* [5]–[11]. These manipulators employ arrays of magnets to generate and flexibly control magnetic fields, which are exploited to manipulate magnetized objects at a distance with no direct contact. The noncontact feature of these manipulators presents a transformative technology for a new generation of minimally invasive medical devices capable of safely operating magnetized surgical tools inside the natural pathways of the patient's body by leveraging external magnetic fields [12]–[18].

Magnetic manipulators conventionally use electromagnets as the source of magnetic field, which are easy to control via their terminal voltages [19]–[23]. Despite this key advantage, electromagnets usually produce much weaker magnetic fields and forces compared to permanent magnets of the same size, weight, and cost [24]. To exploit the stronger magnetic fields of permanent magnets, our research is dedicated to the class of magnetic manipulators that utilize permanent magnets to generate magnetic fields, and control these magnetic fields using electromechanical actuators that dynamically adjust the positions of the permanent magnets.

To validate the early concept of magnetic levitation using permanent magnets, we implemented the conceptual design of Fig. 1 as the experimental setup of Fig. 2. To stabilize this setup, we further designed a linear quadratic regulator (LQR) to implement a stabilizing feedback loop. The procedure of design and development is detailed in Sections II and III for the experimental setup and its stabilizing feedback control, respectively. Section IV presents experimental results, which demonstrate successful levitation of a magnetic object using the developed experimental setup.

II. Basic Concept and Experimental Setup

The schematic diagram of Fig. 1 presents the basic concept of the MLS developed in this paper. The core of this MLS is a magnetomechanical unit consisting of an axially magnetized permanent magnet attached to a linear servomotor, by which, the magnet is moved back and forth inside a nonmagnetic guiding cylinder. This unit is fixed to the rigid frame of the MLS with its magnet facing groundward to attract a magnetic object against the gravity, and consequently, levitate it at a distance from the magnet. The servomotor enables the unit to control its attractive magnetic force by adjusting the distance

This work was supported by the National Science Foundation under Grant No. ECCS-1941944.

D. Basnet was with the School of Electrical, Computer, and Biomedical Engineering, Southern Illinois University. He is currently with Wahl Clipper Corporation, Sterling, IL, 61081 USA (email: dhiraj.basnet@siu.edu).

A. Komaee is with the School of Electrical, Computer, and Biomedical Engineering, Southern Illinois University, Carbondale, IL, 62901 USA (email: akomaee@siu.edu).

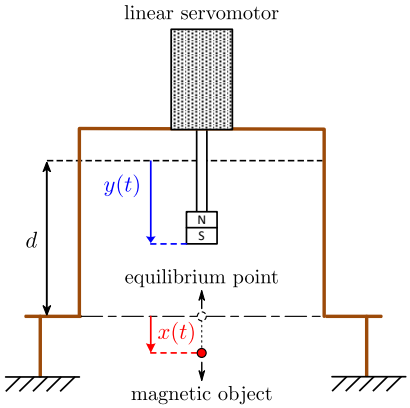

Fig. 1. Conceptual design of a permanent magnet-based MLS proposed in [1], [2] and experimentally verified in this paper. This design incorporates an axially magnetized permanent magnet mounted groundward on a linear servomotor aimed to adjust the distance between the magnet and a levitating magnetic object. This combination provides a controllable magnetic force that balances the gravity at a certain distance from the face of magnet, and consequently levitates a magnetic object at that distance.

between its permanent magnet and the levitating object. The levitating object in this paper is a spherical magnetic bead moving inside a workspace (a container) filled with a viscous fluid. This fluid facilitates the magnetic levitation process by introducing friction to the magnetic bead.

At a certain distance below the face of permanent magnet, its attractive magnetic force applied upward to the levitating object balances the gravity applied downward, which creates an inherently unstable equilibrium point. To sustain magnetic levitation, this equilibrium point must be stabilized using a feedback loop that dynamically controls the magnetic force via the position of the permanent magnet, in turn, controlled by the linear servomotor. This stabilizing control is realized in this work by a linear state feedback designed via the LQR method, and is implemented on a desktop computer equipped with the real-time software LabVIEW. To establish this state feedback, the real-time values of the position and velocity of both the levitating object and permanent magnet are required. These quantities are measured in this work by a high-speed camera and built-in image tracking modules of LabVIEW.

A. *Experimental Setup*

We developed an experimental setup realizing a benchtop MLS based on the conceptual design of Fig. 1. This MLS and its main components are shown in Fig. 2. These components include a permanent magnet actuated by a linear servomotor inside a guiding cylinder, a workspace containing a levitating magnetic bead, and a camera with an adjustable mount. As shown in Fig. 2(e), all these components were installed on a rigid frame to form a benchtop MLS. This rigid frame, the guiding cylinder for the permanent magnet (also housing the servomotor), and the adjustable camera mount were designed individually using SolidWorks and fabricated by 3D printing. The structure and design of the building blocks composing the developed MLS are discussed below. For a more detailed discussion, the reader is referred to [3].

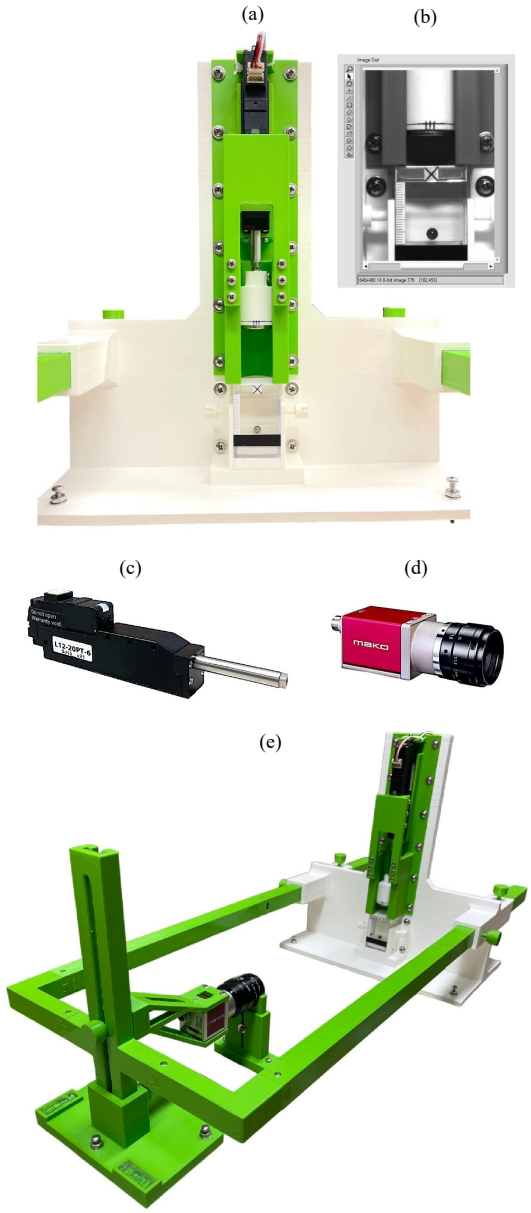

Fig. 2. Experimental setup implementing the conceptual design of Fig 1 for magnetic levitation using a permanent magnet and a linear servomotor: (a) front view of the prototyped MLS; (b) levitating magnetic object inside its workspace filled with a transparent viscous fluid; (c) linear servomotor; (d) camera for position tracking; (e) overall setup including the camera and its adjustable mount. The permanent magnet is housed in a rigid holder (the cylinder in (a) colored in white) attached to the servomotor and can freely move inside a vertical guiding cylinder. The image in (b) is a single frame captured by the camera, from which the positions of the levitating object and the permanent magnet are extracted in real time.

1) Magnetomechanical Unit: The main building block of the developed MLS is an apparatus consisting of a cylindrical magnet bar attached to the rod end of the linear servomotor of Fig. 2(c), both housed in a rigid structure fabricated by 3D printing (the part in Fig. 2(a) colored in green). The magnet bar is a grade N52 neodymium iron boron (NdFeB) cylinder of diameter and length 25.4 mm, which is magnetized axially. The servomotor is a mightyZAP model L12-20PT-6 with the

maximum load of 34 N, maximum speed of 80 mm/sec, and a stroke of 56 mm. The servomotor is coupled to the magnet by a 3D-printed connector that houses the magnet in one side and connects to the servomotor from another side (appears in Fig. 2(a) in white color).

The servomotor is interfaced to the desktop computer (the computer used for feedback control) by an 8-bit Atmega2560 microcontroller, operating the servomotor in its pulse width modulation (PWM) mode. This microcontroller is connected to the desktop computer by a USB Type-A to USB Type-B cable, communicates with LabVIEW through the Universal Asynchronous Receiver Transmitter (UART) communication protocol, and is programmed offline using Atmel Studio.

2) Workspace and Levitating Object: The workspace is a transparent $32 \times 30 \times 30$ mm container housed tightly in a holder fabricated just below the magnetomechanical unit, as shown Fig. 2(a). This container is filled with light corn syrup and houses a nickel coated steel bead as a levitating object. The steel bead is a sphere of 5 mm diameter and 7800 kg/m^3 density, and has a magnetic susceptibility of 1000. The corn syrup is transparent and has a viscosity of around 4750 cP. To prevent evaporation of water from the corn syrup, which changes its viscosity, the container is tightly sealed.

3) Camera and Its Adjustable Mount: The optical camera in Fig. 2(d) is utilized for real-time tracking of the positions of both the levitating object and the permanent magnet. These quantities are estimated in real time by the Vision Assistant module of LabVIEW by extracting information from images captured by the camera at the rate of 60 fps and the resolution of 640×480 pixels. An instance of such images is shown in Fig. 2(b). To focus the camera properly on the workspace and its nearby permanent magnet, it is installed on a 3D-printed adjustable mount, which is rigidly attached to the structure of the developed MLS. This camera mount is able to adjust the distance and height of the camera from the workspace.

The camera selected in this work is a monochrome Allied Vision Mako U-029B with a CMOS ON Semi PYTHON 300 image sensor. It is connected to the desktop computer via a USB 3.0 cable, and is accessed by LabVIEW using its Vision Acquisition Express module.

B. Real-Time Computation

The real-time computation required to realize a stabilizing feedback control is performed by LabVIEW. Two major tasks are undertaken by this computation: servomotor control and image tracking. For servomotor control, the numerical values of the linear control law (8), developed in Section III-B, are computed and sent to the Atmega2560 microcontroller to run the servomotor. This control law is a state feedback expressed in terms of the positions and velocities of the levitating object and the permanent magnet, which are estimated from images captured by the camera. The estimation process is the second task of real-time computation.

In the first step of this process, both positions are estimated via a pattern matching algorithm implemented by the Vision Assistant module of LabVIEW. Viewed as functions of time, the estimated positions turned out to contain substantial noise due to such factors as camera vibrations and flickering light sources. This noise is suppressed via low-pass filtering before involving the estimated positions in computation of control. The velocities of the levitating object and permanent magnet are constructed by numerically differentiating their positions with respect to time using the derivative block of LabVIEW.

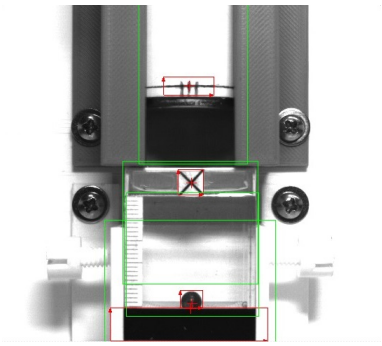

Fig. 3. Image calibration procedure.

C. Image Calibration for Position Tracking

To utilize the pattern matching algorithm of LabVIEW, an *image calibration* procedure must be implemented, which is explained below using Fig. 3. This algorithm scans an image to locate specific patterns in that image, and then report their positions with respect to some coordinate system. For the purpose of this paper, the algorithm identifies the levitating object (steel bead) with its round shape boxed in red in Fig. 3. Similarly, the permanent magnet is recognized by the sign ||| printed on the tip of its holder. The algorithm reports the vertical positions of these objects with respect to a point on top of the workspace marked by a $\times$ sign. A dark strip across the bottom of workspace (see Fig. 3) is used for calibration of length scale, knowing that the actual hight of the workspace is 32 mm.

III. System Dynamics and Control Design

To stabilize the experimental setup described in Section II, a feedback control law is designed in this section based on a set of state-space equations governing its dynamics. These equations are presented in Section III-A without details on their derivation, since such details can be accessed in [1]. The stabilizing feedback law is developed in Section III-B, and a procedure for its tuning is offered in Section III-C.

A. System Dynamics

The dynamics of the MLS schematically shown in Fig. 1 is represented by four state variables: the position $x(t)$ and velocity $v_x(t)$ of the levitating object, and the position $y(t)$ and velocity $v_y(t)$ of the permanent magnet. As shown in Fig. 1, the position of the levitating object is measured with respect to the equilibrium point at which it must be levitated, and along a vertical vector directed toward the ground. The permanent magnet is located along the same vector, but with respect to a reference at a distance d above the equilibrium point (the significance of d is explained later).

The control input $u(t)$ to the overall MLS is the reference signal to the linear servomotor, which controls the position of its rod end, and thereby, the position $y(t)$ of the permanent magnet. This reference input is calibrated in such a manner that $y(t)$ closely tracks $u(t)$ to ideally hold $y(t) = u(t)$. In practice however, the relationship between $y(t)$, as an output, and $u(t)$ as an input is governed by a second-order linear[1] dynamics represented by the transfer function

$$H(s) = \frac{\omega_n^2}{s^2 + 2\zeta\omega_n s + \omega_n^2}. \tag{1}$$

Here, ω_n and ζ are positive constants known as the natural frequency and damping ratio of the servomotor, respectively.

The dynamics of the MLS in Fig. 1 is described in [1] by the set of nonlinear state-space equations

$$\dot{x}(t) = v_x(t) \tag{2a}$$
$$\dot{v}_x(t) = -\sigma v_x(t) + a\big(x(t) - y(t)\big) \tag{2b}$$
$$\dot{y}(t) = v_y(t) \tag{2c}$$
$$\dot{v}_y(t) = -2\zeta\omega_n v_y - \omega_n^2 y(t) + \omega_n^2 u(t). \tag{2d}$$

Among these equations, (2a) reflects the trivial relationship between position and velocity of the levitating object, and the pair (2c)-(2d) represents the transfer function (1) in the time domain. The state equation (2b) is an end result of Newton's second law, describing the motion of a magnetic object under an upward magnetic force, the downward gravity, and the Stokes drag force acting against the motion as it moves inside a viscous fluid. This equation is discussed in more detail next.

The magnetic object is a sphere of radius r and mass m, the viscosity of fluid is η, and the gravitational acceleration is denoted by g. The magnetic force is a function $F_m(w)$ that depends on the distance w between the magnetic object and the permanent magnet. It is assumed that d is a distance from the face of magnet at which the magnetic force is equal to the gravitational force mg, i.e., d solves the algebraic equation

$$\frac{F_m(d)}{m} = g. \tag{3}$$

Then, the magnetic force applied to the magnetic object at time t is given by $F_m\big(x(t) - y(t) + d\big)$. Moreover, the Stokes drag is known [21] to be $6\pi r\eta v_x(t)$. Newton's second law of motion implies that

$$m\dot{v}_x(t) = -6\pi r\eta v_x(t) + mg - F_m\big(x(t) - y(t) + d\big),$$

which can be rewritten as (2b) by defining the scaler function

$$a(z) = g - \frac{F_m(z+d)}{m} \tag{4}$$

and the positive constant

$$\sigma = \frac{6\pi r\eta}{m}. \tag{5}$$

The permanent magnet in this work is axially symmetric, and the magnetic field (in Tesla) along its axis of symmetry at the distance w from its face is denoted by $B(w)$. At the distance w along its axis of symmetry, this magnet applies a magnetic force $F_m(w)$ to a small magnetic object, which is expressed in terms of $B(w)$ as [21]

$$F_m(w) = \frac{m}{2\rho\mu_0} \cdot \frac{\chi}{1 + \chi/3} \cdot \frac{d}{dw} B^2(w). \tag{6}$$

Here, m, ρ, and χ are the mass, the density, and the magnetic susceptibility of the magnetic object, respectively, and μ_0 is the permeability of free space.

B. Control Design

The state-space equations (2) are inherently nonlinear as a result of the nonlinear function $a(\cdot)$ appearing in (2b). To stabilize the nonlinear dynamics of the developed MLS, a simple approach is to develop a linear controller based on an approximate model derived from (2) by linearizing it around its equilibrium point. Even though this approach may not be as effective as more advanced methods such as the feedback linearization we proposed in [1], it is adopted in this work as a reliable early step.

It can be readily concluded from (3) and (4) that $a(0) = 0$, which in turn implies that $(x, v_x, y, v_y) = (0, 0, 0, 0)$ is an equilibrium point of the nonlinear state-space equations (2). Then, application of the linear approximation $a(z) \simeq a'(0)\, z$ to the nonlinear state equation (2b) results in the linear model

$$\dot{x}(t) = v_x(t) \tag{7a}$$
$$\dot{v}_x(t) = -\sigma v_x(t) + a'(0)\big(x(t) - y(t)\big) \tag{7b}$$
$$\dot{y}(t) = v_y(t) \tag{7c}$$
$$\dot{v}_y(t) = -2\zeta\omega_n v_y(t) - \omega_n^2 y(t) + \omega_n^2 u(t) \tag{7d}$$

to approximate the dynamics of the developed MLS. It can be verified that for any valid set of parameter values (i.e., for positive σ, $a'(0)$, ω_n, and ζ), this dynamics is unstable with exactly one positive eigenvalue.

This unstable dynamics is stabilized in this paper using a linear state feedback of the form

$$u(t) = -\big(k_1 x(t) + k_2 v_x(t) + k_3 y(t) + k_4 v_y(t)\big) \tag{8}$$

with a gain vector (k_1, k_2, k_3, k_4) tuned via the LQR method. This method guarantees the closed-loop stability of the linear system (7) under the linear state feedback (8) by choosing the gain vector in such a manner to minimize the quadratic cost

$$J = \int_0^\infty \Big(q_1 x^2(t) + q_2 v_x^2(t) + q_3 y^2(t) + q_4 v_y^2(t) + u^2(t)\Big) dt. \tag{9}$$

Here, q_1, q_2, q_3, and q_4 are nonnegative design parameters, properly chosen for the best closed-loop performance.

C. Control Tuning

Once the model parameters $(\sigma, a'(0), \omega_n, \zeta)$ in (7) and the design parameters (q_1, q_2, q_3, q_4) in (9) are determined, the gain vector (k_1, k_2, k_3, k_4) can be easily obtained by the `lqr` function of MATLAB. For the servomotor parameters, the numerical values $\omega_n = 39.8$ rad/sec and $\zeta = 0.7$ have been

[1] In [1], this linear model is modified to reflect the nonlinear effects caused by finite speed of the servomotor. The modifications are not applied here, since the maximum speed of the servomotor is not exceeded in this work.

Fig. 4. Senis MMS-1A-RS magnetic field scanner. This instrument provides a platform for measurement and empirical modeling of magnetic fields. It consists of a holder for accommodating magnets, a 3D manipulator which can scan a volume of $135 \times 135 \times 135$ mm around the magnets with 1 μm spatial resolution, and a 3D magnetic sensor on the tip of the manipulator, which can measure a vector of magnetic field with 0.1% accuracy.

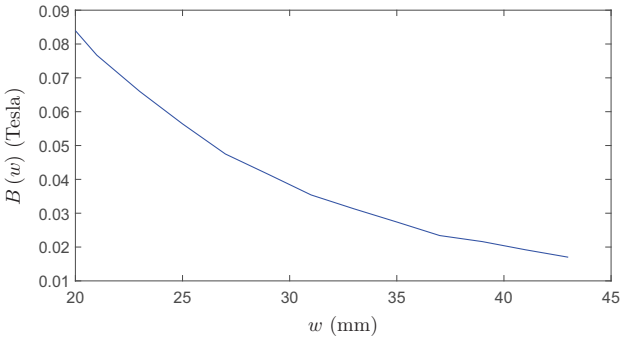

Fig. 5. Axial component of magnetic field along the axis of symmetry of a grade N52 NdFeB magnet, illustrated versus the distance w from its face.

estimated in [1] using experiments and system identification techniques. These values are identically adopted in this paper. The numerical value $\sigma = 438.7$ was computed from (5) for a magnetic bead of radius $r = 2.5$ mm and mass $m = 0.51$ gm, and a fluid of viscosity $\eta = 4.75$ Pa.sec. The numerical value of $a'(0) = 1685.5$ was computed from

$$a'(0) = -\frac{1}{m} \cdot \frac{d}{dw} F_m(w) \Big|_{w=d}$$

in terms of d in (3) and the magnetic force $F_m(w)$, both constructed via the following experimental procedure.

At first, the axial component $B(w)$ of magnetic field was measured along the axis of symmetry of a grade N52 NdFeB magnet bar, ranging from 20 mm to 45 mm from its face. The measurements were performed by a Senis MMS-1A-RS magnetic field scanner, shown in Fig. 4. The recorded results of measurement are shown in the graph of Fig. 5. By numeric differentiation of this graph, the magnetic force $F_m(w)$ was next constructed using (6) for $\rho = 7800$ kg/m^3, $\chi = 1000$, and $\mu_0 = 4\pi \times 10^{-7}$ H/m. The resulting graph of magnetic acceleration (magnetic force per unit of mass) is illustrated in Fig. 6, from which, the numerical value of $d = 37.5$ mm was extracted according to (3).

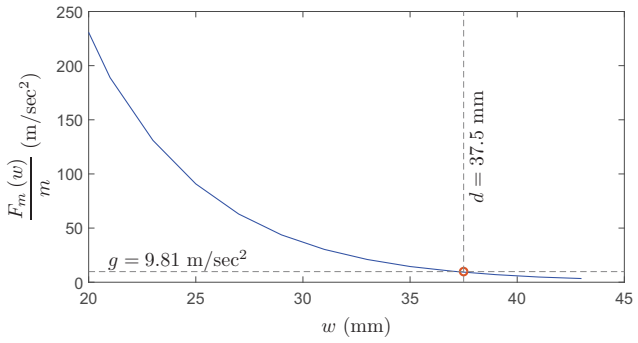

Fig. 6. Experimentally computed magnetic acceleration (magnetic force per unit of mass) for an N52 NdFeB magnet versus distance from its face. At a distance $d = 37.5$ mm from the face of magnet, the magnetic acceleration is equal to the gravitational acceleration $g = 9.81$ m/sec^2.

With the knowledge of model parameters, suitable values of the design parameters (q_1, q_2, q_3, q_4) were determined by experiments. In each experiment, new values for the design parameters were guessed, their associated LQR gain vector was implemented on the experimental setup, and the control performance was observed in practice and evaluated against previous experiments. By learning from each experiment and iteratively improving the gain vector, the best performance was attained under $(q_1, q_2, q_3, q_4) = (800, 100, 100, 100)$ and

$$(k_1, k_2, k_3, k_4) = (-140.76, -0.36, 109.74, 9.98). \quad (10)$$

The control performance for this gain vector is reported next.

IV. Experimental Validation

A feedback loop with the gain values (10) was established to stabilize the developed MLS. The successful operation of this feedback loop is verified by Fig. 7, in which a magnetic bead is levitated against gravity inside the workspace of the MLS. The graph of Fig. 8 illustrates the position $x(t)$ of the magnetic bead versus time during the levitation process, starting at $t = 0$. As shown in this figure, the magnetic bead is initially at $x(0) \simeq 3$ mm (i.e., 3 mm below its equilibrium point), and within about 10 seconds, it reaches the steady state with an error of ± 0.08 mm from the equilibrium point.

As observed in Fig. 8, this error appears in the steady-state regime as sustained oscillations around the equilibrium point. The exact source of these oscillations is not known; yet, the most likely cause is the gear backlash or other imperfections that limit the resolution of the servomotor in use. Some other potential causes include: PWM actuation of the servomotor, finite resolution of camera, which in turn results in finite resolution of position estimates, and vibrations of the MLS structure resulting in jittery position estimates.

It is observed in Fig. 8 that the stabilizing feedback loop has a relatively long settling time about 10 sec, which indeed, is a manifestation of its low bandwidth caused by the high viscosity of the fluid inside workspace. The settling time can be shortened either by increasing the feedback gain (stronger feedback loop) or by reducing the viscosity. In either case, a larger maximum speed of the servomotor will be required,

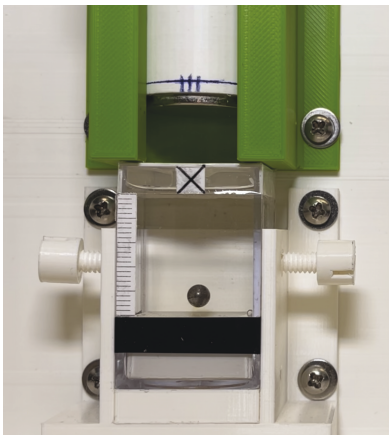

Fig. 7. Magnetic object successfully levitated by the developed MLS.

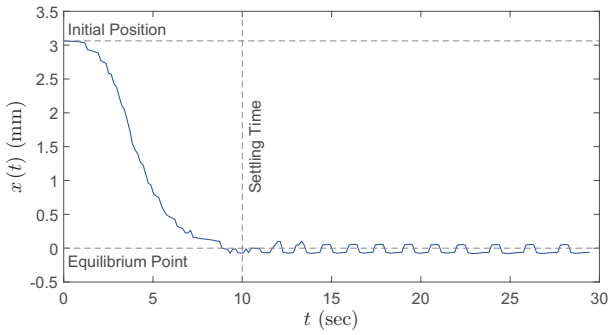

Fig. 8. Position of the magnetic bead versus time during the levitation process ($0 \leqslant t \leqslant 10$ sec), and after its completion ($t > 10$ sec).

which can be beyond the capacity of the servomotor currently in use. Therefore, to decrease the settling time, a stronger servomotor with a higher maximum speed is necessary.

V. Conclusion

The idea of magnetic levitation using permanent magnets was validated by experiments on a benchtop MLS consisting of an axially magnetized permanent magnet bar and a linear servomotor. Using a computer-based feedback controller, the benchtop MLS was successfully stabilized in order to levitate a magnetic bead around an equilibrium point at which the net force applied upward to the magnetic bead by the permanent magnet and downward by the gravity is zero. The results of this paper contribute to the development of a new generation of more efficient magnetic manipulators which replace large, heavy, expensive, and energy consuming electromagnets with permanent magnets and electromechanical actuators.

References

[1] M. R. Shariatmadari and A. Komaee, "Feedback stabilization of a permanent magnet levitation system," in *Proc. of the 2022 American Control Conference (ACC 2022)*, pp. 5087–5092, 2022.

[2] M. R. Shariatmadari, "Feedback control and stability analysis of a permanent magnet levitation system," Master's thesis, Southern Illinois University, Carbondale, 2021.

[3] D. Basnet, "Design, implementation, and feedback stabilization of a permanent magnet levitation system," Master's thesis, Southern Illinois University, Carbondale, 2023.

[4] M. B. Khamesee, N. Kato, Y. Nomura, and T. Nakamura, "Design and control of a microrobotic system using magnetic levitation," *IEEE/ASME Trans. Mechatronics*, vol. 7, no. 1, pp. 1–14, 2002.

[5] N. Riahi and A. Komaee, "Steering magnetic particles by feedback control of permanent magnet manipulators," in *Proc. of 2019 American Control Conference (ACC 2019)*, pp. 5432–5437, 2019.

[6] N. Riahi, L. R. Tituaña, and A. Komaee, "Homotopy continuation for feedback linearization of noncontact magnetic manipulators," in *Proc. of 2020 American Control Conference (ACC 2020)*, pp. 4295–4300, 2020.

[7] N. Riahi and A. Komaee, "Noncontact steering of magnetic objects by optimal linear feedback control of permanent magnet manipulators," in *Proc. of 2020 IEEE/ASME International Conference on Advanced Intelligent Mechatronics (AIM 2020)*, pp. 30–35, 2020.

[8] L. R. Tituaña, "Implementation of a planar magnetic manipulator with rotatable permanent magnets," Master's thesis, Southern Illinois University, Carbondale, 2020.

[9] M. Mohammadzadeh, M. R. Shariatmadari, N. Riahi, and A. Komaee, "Feedback decoupling of magnetically coupled actuators," in *Proc. of the 2021 IEEE/ASME International Conference on Advanced Intelligent Mechatronics (AIM 2021)*, pp. 320–325, 2021.

[10] T.-A. Sneed and A. Komaee, "Nonparametric reconstruction of vector fields from noisy observations of their flow curves," in *Proc. of the 2021 American Control Conference (ACC 2021)*, pp. 3959–3964, 2021.

[11] N. Riahi, *Design, Optimization, and Feedback Control of a Planar Noncontact Magnetic Manipulator With Rotatable Permanent Magnets*. PhD thesis, Southern Illinois University, Carbondale, 2021.

[12] M. Sendoh, K. Ishiyama, and K.-I. Arai, "Fabrication of magnetic actuator for use in a capsule endoscope," *IEEE Trans. Magn.*, vol. 39, no. 5, pp. 3232–3234, 2003.

[13] G. Ciuti, P. Valdastri, A. Menciassi, and P. Dario, "Robotic magnetic steering and locomotion of capsule endoscope for diagnostic and surgical endoluminal procedures," *Robotica*, vol. 28, no. 2, pp. 199–207, 2010.

[14] M. Simi, P. Valdastri, C. Quaglia, A. Menciassi, and P. Dario, "Design, fabrication, and testing of a capsule with hybrid locomotion for gastrointestinal tract exploration," *IEEE/ASME Trans. Mechatronics*, vol. 15, no. 2, pp. 170–180, 2010.

[15] S. Yim and M. Sitti, "Design and rolling locomotion of a magnetically actuated soft capsule endoscope," *IEEE Trans. Robot.*, vol. 28, no. 1, pp. 183–194, 2012.

[16] M. Beccani, C. Di Natali, L. J. Sliker, J. A. Schoen, M. E. Rentschler, and P. Valdastri, "Wireless tissue palpation for intraoperative detection of lumps in the soft tissue," *IEEE Trans. Biomed. Eng.*, vol. 61, no. 2, pp. 353–361, 2014.

[17] V. Iacovacci, L. Ricotti, P. Dario, and A. Menciassi, "Design and development of a mechatronic system for noninvasive refilling of implantable artificial pancreas," *IEEE/ASME Trans. Mechatronics*, vol. 20, no. 3, pp. 1160–1169, 2015.

[18] L. Sliker, G. Ciuti, M. Rentschler, and A. Menciassi, "Magnetically driven medical devices: a review," *Expert Review of Medical Devices*, vol. 12, no. 6, pp. 737–752, 2015.

[19] E. G. Quate, K. G. Wika, M. A. Lawson, G. T. Gillies, R. C. Ritter, M. S. Grady, and M. A. Howard, "Goniometric motion controller for the superconducting coil in a magnetic Stereotaxis system," *IEEE Trans. Biomed. Eng.*, vol. 38, no. 9, pp. 899–905, 1991.

[20] M. P. Kummer, J. J. Abbott, B. E. Kratochvil, R. Borer, A. Sengul, and B. J. Nelson, "OctoMag: An electromagnetic system for 5-DOF wireless micromanipulation," *IEEE Trans. Robot.*, vol. 26, no. 6, pp. 1006–1017, 2010.

[21] R. Probst, J. Lin, A. Komaee, A. Nacev, Z. Cummins, and B. Shapiro, "Planar steering of a single ferrofluid drop by optimal minimum power dynamic feedback control of four electromagnets at a distance," *J MAGN MAGN MATER*, vol. 323, no. 7, pp. 885–896, 2011.

[22] A. Komaee and B. Shapiro, "Steering a ferromagnetic particle by optimal magnetic feedback control," *IEEE Trans. Control Syst. Technol.*, vol. 20, no. 4, pp. 1011–1024, 2012.

[23] S. Afshar, M. B. Khamesee, and A. Khajepour, "Optimal configuration for electromagnets and coils in magnetic actuators," *IEEE Trans. Magn.*, vol. 49, no. 4, pp. 1372–1381, 2013.

[24] O. Baun and P. Blümler, "Permanent magnet system to guide superparamagnetic particles," *J MAGN MAGN MATER*, vol. 439, pp. 294–304, 2017.